Dissociative recombination and rotational transitions of D+2 in collisions with slow electrons

M. D. Epée Epée, O. Motapon, N. Pop, F. Iacob, E. Roueff, I. F. Schneider, J. Zs Mezei

Monthly Notices of the ROYAL ASTRONOMICAL SOCIETY

MNRAS **512,** 424–429 (2022) https://doi.org/10.1093/mnras/stac501
Advance Access publication 2022 February 25

Dissociative recombination and rotational transitions of D_2^+ in collisions with slow electrons

M. D. Epée Epée,[1] O. Motapon,[1,2] N. Pop,[3] F. Iacob,[4] E. Roueff,[5] I. F. Schneider[6,7] and J. Zs. Mezei[6,8]★

[1]*Department of Physics, Faculty of Sciences, University of Douala, P. O. Box 24157, Douala, Cameroon*
[2]*Faculty of Science, University of Maroua, P. O. Box 814, Maroua, Cameroon*
[3]*Department of Physical Foundation of Engineering, University Politechnica of Timisoara, 300223, Timisoara, Romania*
[4]*Physics Faculty, West University of Timisoara, 300223,Timisoara, Romania*
[5]*LERMA, Observatoire de Paris, PSL Research University, CNRS, Sorbonne Universités, 92190, Meudon, France*
[6]*LOMC CNRS-UMR6294, Université le Havre Normandie, F-76058 Le Havre, France*
[7]*LAC CNRS-FRE2038, Université Paris-Saclay, F-91405 Orsay, France*
[8]*Institute for Nuclear Research (ATOMKI), H-4001 Debrecen, Hungary*

Accepted 2022 February 20. Received 2022 February 20; in original form 2022 January 11

ABSTRACT

Rate coefficients for dissociative recombination and state-to-state rotational transitions of the D_2^+ ion induced by collisions with very low-energy electrons have been reported following our previous studies on HD^+ and H_2^+. The same molecular structure data sets, excitations ($N_i^+ \rightarrow N_f^+ = N_i^+ + 2$ for $N_i^+ = 0$ to 10) and de-excitations ($N_i^+ \rightarrow N_f^+ = N_i^+ - 2$, for $N_i^+ = 2$ to 10) were used for collision energies ranging from 0.01 meV to 0.3 eV. Isotopic effects for dissociative recombination and rotational transitions of the vibrationally relaxed targets are presented.

Key words: ISM: abundances – ISM: kinematics and dynamics – ISM: molecules – molecular processes – scattering.

1 INTRODUCTION

Among many 'cold' ionized environments, in the diffuse interstellar media and planetary atmospheres, electrons are presumed to be one of the most important exciting species for molecular cations. Recent studies based on astrophysical observations and calculations regarding diatomic and polyatomic molecular charged species (Faure & Tennyson 2001, 2002, 2003; Faure et al. 2006; Kokoouline et al. 2010) show that the cross-sections of electron impact rotational transitions of molecular cations significantly exceed those obtained by atomic and/or molecular impact.

At very low electron collision energy, the electron impact-induced rotational transitions of the vibrationally relaxed molecular cations

$$AB^+(N_i^+, v_i^+ = 0) + e^-(\varepsilon) \longrightarrow AB^+(N_f^+, v_f^+ = 0) + e^-(\varepsilon') \quad (1)$$

are in strong competition with the dissociative recombination (DR):

$$AB^+(N_i^+, v_i^+ = 0) + e^-(\varepsilon) \longrightarrow A + B, \quad (2)$$

here N_i^+/N_f^+ and v_i^+/v_f^+ stand for the initial/final rotational and vibrational quantum numbers of the cation and ε/ε' the kinetic energy of the incident/scattered electrons.

Recently, in the Le Havre group, several studies were performed on the electron-induced reactions of H_2^+ and HD^+ (Motapon et al. 2008; Waffeu Tamo et al. 2011; Chakrabarti et al. 2013; Motapon et al. 2014; Epée et al. 2016; Djuissi et al. 2020). State-to-state cross-sections and rate coefficients were reported for ro-vibrational transitions including inelastic collisions ($N_i^+ < N_f^+$ and/or $v_i^+ < v_f^+$), superelastic collisions ($N_i^+ > N_f^+$ and/or $v_i^+ > v_f^+$), DR, and – at high collision energies – dissociative excitation (DE).

The calculations were performed within the framework of our stepwise multichannel quantum defect theory (MQDT, Giusti-Suzor 1980; Mezei et al. 2019, and references therein).

These results were compared with experimental results obtained for HD^+ and H_2^+ on different merged beam (Auerbach et al. 1977; Hus et al. 1988) and storage ring experiments performed at the Heidelberg Test Storage Ring (Krohn et al. 2000; Krohn 2001; Shafir et al. 2009; Schwalm et al. 2011) and the Aarhus Astrid Storage Ring (Andersen et al. 1997). The calculated cross-sections and rate coefficients agree satisfactorily with the measured ones for both DR and ro-vibrational excitation processes.

It is also interesting to report that simple deuterium chemistry has been suggested to take place in the primordial conditions, where essentially only Hydrogen, Deuterium, and Helium elements are present (Lepp & Shull 1984). The presence of HD, with its small permanent dipole moment, may indeed contribute to the cooling of the medium. Several groups have explicitly introduced coupled Hydrogen/Deuterium/Helium chemistry as emphasized in the review paper of Galli & Palla (2013). However, to our knowledge, only Gay et al. (2011) have explicitly introduced multiple deuterated compounds in this context, including D_2^+, HD_2^+, and D_3^+ and conclude their paper by emphasizing the large uncertainties present in their deuterium chemistry and claim for additional studies on the topic. As an example, they suggest that the DR rate coefficient of D_2^+ is equal to $1.2 \times 10^{-8}(\frac{T}{300})^{-0.4}$, which is equal to their estimate of the H_2^+ DR rate coefficient. The aim of this study is to overcome that assumption and to explicitly consider the different nuclear effects for the DR of the heavy D_2^+ molecular ion, as a natural extension of

★ E-mail: mezei.zsolt@atomki.hu

previous studies on H_2^+ and HD^+ (Motapon et al. 2014; Epée et al. 2016).

The paper is organized as follows. In Section 2, we briefly describe our theoretical approach. Rate coefficients and their comparison with previous results are presented in Section 3, and the conclusions follow in Section 4.

2 THEORETICAL METHOD

The efficiency of our theoretical method in modelling the electron/diatomic cation collisions, based on the stepwise MQDT, has been proved in many previous studies on different species, including H_2^+ and its isotopologues (Motapon et al. 2008; Waffeu Tamo et al. 2011; Chakrabarti et al. 2013; Motapon et al. 2014; Epée et al. 2016; Djuissi et al. 2020), CH^+ (Mezei et al. 2019), SH^+ (Kashinski et al. 2017), etc. The general ideas of our approach were already presented in detail many times, see for example Mezei et al. (2019) and, therefore, here we restrict ourselves to its major steps.

The equations (1) and (2) involve *ionization* channels – characterizing the scattering of an electron on the target cation – and *dissociation* channels – relating to atom–atom scattering. The mixing of these channels results in quantum interference of the *direct* mechanism – in which the capture takes place into a doubly excited dissociative state of the neutral system – with the *indirect* one – in which the capture occurs via a Rydberg bound state of the molecule belonging to a *closed* channel, this state being pre-dissociated by the dissociative one. In both mechanisms the auto-ionization – based on the existence of *open* ionization channels – is in competition with the pre-dissociation, and can lead to the excitation or to the de-excitation of the cation.

More specifically, each of the ionization channels, built by adding an electron to the D_2^+ ion in its ground electronic state $X^2\Sigma_g^+$ in a particular vibrational level, interacts with all the dissociation exit channels (Rydberg-valence interaction) for all the relevant symmetries ($^1\Sigma_g^+$, $^1\Pi_g$, $^1\Delta_g$, $^3\Sigma_g^+$, $^3\Pi_g$, $^3\Delta_g$, $^3\Sigma_u^+$, and $^3\Pi_u$). Depending on the total energy of the system these ionization channels can be *open* – either as entrance channels, describing the incident electron colliding the ion in its ground electronic state, or exit channels, describing the auto-ionization, i.e. resonant elastic scattering, rovibrational excitation, and de-excitation – or *closed* – describing the resonant temporary captures into Rydberg states.

The MQDT treatment of DR and rotational transitions requires the a priori knowledge of the potential energy curves of the ion ground state and the relevant doubly excited, dissociative states of the neutral molecule, as well as for the Rydberg series of mono-excited states represented by the quantum defects. The driving forces of the recombination and excitation processes are the electronic couplings that connect the dissociative and ionization continua.

At low collision energies, besides the type of the crossing of the neutral states with the ground ion state (favourable or less favourable crossing), the rotational couplings among the neutral states with different symmetries are of key importance (Motapon et al. 2014). In our calculations, the $^1\Sigma_g^+$ symmetry rotationally couples to $^1\Pi_g$ and $^1\Delta_g$, $^3\Sigma_g^+$ couples to $^3\Pi_g$ and $^3\Delta_g$, and, finally, $^3\Sigma_u^+$ couples to $^3\Pi_u$. For the remaining symmetries the electronic couplings are for at least two orders of magnitude smaller so they can be neglected. Most of these data were extracted from *ab initio* molecular structure calculations of Wolniewicz et al. (Kolos & Wolniewicz 1969; Wolniewicz & Dressler 1994; Orlikowski, Staszewska & Wolniewicz 1999; Staszewska & Wolniewicz 2002), completed by R-matrix calculations of Tennyson (1996) and Telmini & Jungen (2003). For each of the symmetries involved, only the lowest dissociative states are considered since they are the relevant ones in low-energy collisions. As for the ionization channels, the partial waves considered for the incident electron were s and d for the $^1\Sigma_g^+$ states, d for $^1\Pi_g$, $^1\Delta_g$, $^3\Sigma_g^+$, $^3\Pi_g$ and $^3\Delta_g$, and p waves for $^3\Sigma_u^+$ and $^3\Pi_u$.

The first step in our approach is to build the *interaction matrix* $\mathcal{V}$ that drives the collision, whose elements quantify the couplings between the different channels – ionization and dissociation ones.

Once the $\mathcal{V}$-matrix is built, we construct the short-range reaction matrix $\mathcal{K}$ of the collision, as a second-order perturbative solution of the Lippmann–Schwinger equation. The diagonalized version of the $\mathcal{K}$-matrix (in the eigenchannel representation) whose eigenvalues are expressed in terms of long-range phase-shifts of the eigenfunctions, together with the vibronic couplings between the ionization channels, serve for the building of the frame transformation matrices.

Applying a Cayley transformation on these latter matrices we can set up the generalized scattering matrix $\mathbf{X}$. The Seaton's method of 'eliminating' the closed channels (Seaton 1983) is then employed, resulting in the physical scattering matrix $\mathbf{S}$:

$$\mathbf{S} = \mathbf{X}_{oo} - \mathbf{X}_{oc}\frac{1}{\mathbf{X}_{cc} - \exp(-\mathrm{i}2\pi\nu)}\mathbf{X}_{co}\,, \tag{3}$$

relying on the block-matrices involving open ($\mathbf{X}_{oo}$), open and closed ($\mathbf{X}_{oc}$ and $\mathbf{X}_{co}$), and closed ($\mathbf{X}_{cc}$) channels. The diagonal matrix $\boldsymbol{\nu}$ in the denominator of equation (3) contains the effective quantum numbers corresponding to the vibrational thresholds of the closed ionization channels at given total energy of the system.

Finally, the global cross-section for the DR and for the rotational transitions – rotational excitation/de-excitation (RE/RdE) and resonant elastic scattering of a vibrationally relaxed ion reads as

$$\sigma_{\mathrm{diss}\leftarrow N_i^+} = \sum_{\Lambda,\mathrm{sym}}\frac{\pi}{4\varepsilon}\rho^{(\mathrm{sym},\Lambda)}\sum_N\frac{2N+1}{2N_i^++1} \times\sum_{l,j}\mid S^{(\mathrm{sym},\Lambda,N)}_{d_j,N_i^+l}\mid^2, \tag{4}$$

and

$$\sigma_{N_f^+\leftarrow N_i^+} = \sum_{\Lambda,\mathrm{sym}}\frac{\pi}{4\varepsilon}\rho^{(\mathrm{sym},\Lambda)}\sum_N\frac{2N+1}{2N_i^++1} \times\sum_{l,l'}\mid S^{(\mathrm{sym},\Lambda,N)}_{N_f^+l',N_i^+l} - \delta_{N_i^+N_f^+}\delta_{l'l}\mid^2, \tag{5}$$

where sym is referring to the inversion symmetry – gerade/ungerade – and to the spin quantum number of the neutral system, N stands for its total rotational quantum number (for more details see table 1 from Schneider et al. 1997), N_i^+/N_f^+ denote the initial/final rotational quantum number of the cation, and $\rho^{(\mathrm{sym},\Lambda)}$ is the ratio between the multiplicities of the neutral system and of the ion.

The thermal rate coefficients have been obtained by the convolution of the cross-section with the Maxwellian isotropic energy distribution function for the free electrons:

$$\alpha(T) = \frac{2}{kT}\sqrt{\frac{2}{\pi mkT}}\int_0^{+\infty}\sigma(\varepsilon)\varepsilon\exp(-\varepsilon/kT)\mathrm{d}\varepsilon, \tag{6}$$

where m is the mass of the electron, T stands for the temperature, and k is the Boltzmann constant.

3 RESULTS AND DISCUSSIONS

Applying the stepwise MQDT method outlined in the previous section we have calculated the DR (equation 4), and rotational transition (RE and RdE; equation 5) cross-sections of D_2^+ for its lowest 11

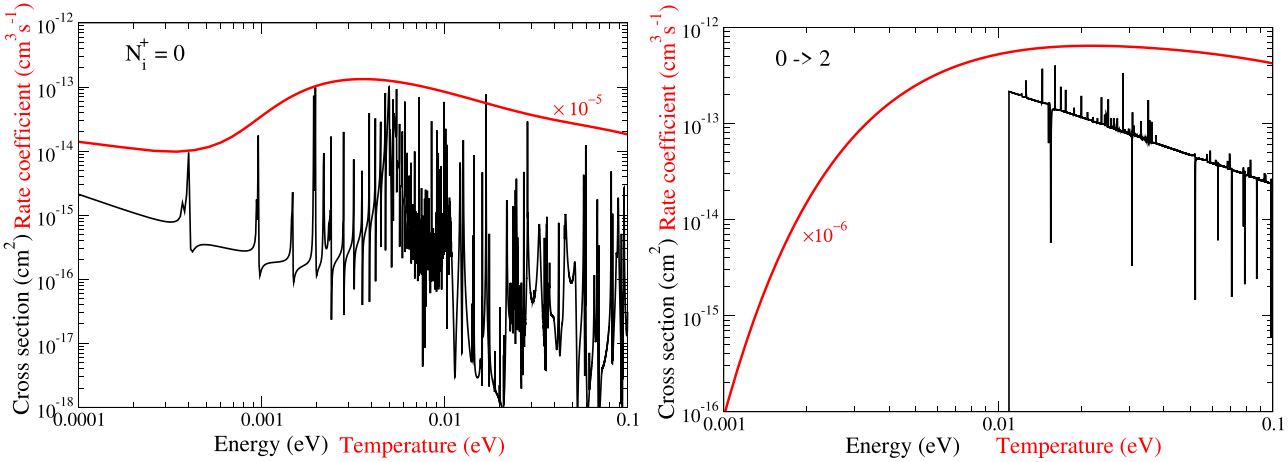

Figure 1. Cross-section (black thin line) and thermal rate coefficient (red thick line) of DR (left-hand panel) and RE (right-hand panel) of ground state D_2^+ (X $^2\Sigma_g^+$, $N_i^+ = 0$, $v_i^+ = 0$). The thermal rate coefficients are scaled by 10^{-5} and 10^{-6}, respectively.

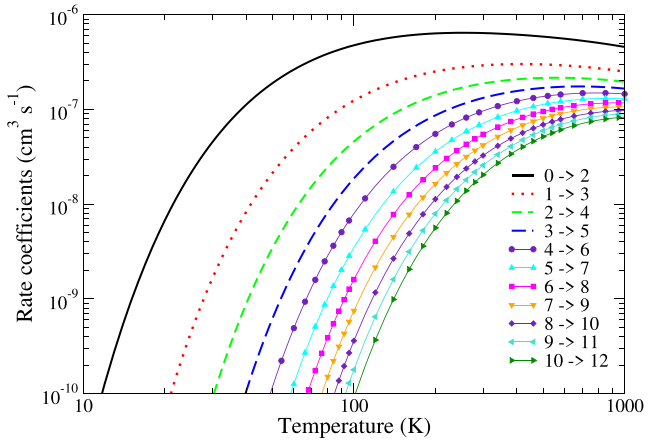

Figure 2. Maxwell rate coefficients for the RE $N_i^+ \rightarrow N_f^+ = N_i^+ + 2$, with $N_i^+ = 0$ to 10 of the vibrationally relaxed ($v_i^+ = 0$) D_2^+ (X $^2\Sigma_g^+$).

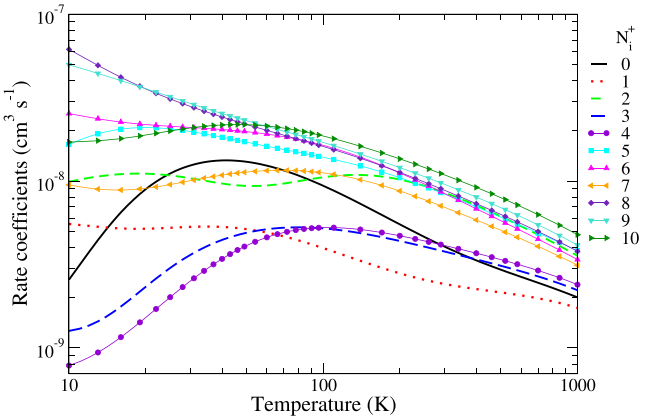

Figure 3. Maxwell rate coefficients for the DR of D_2^+ (X $^2\Sigma_g^+$, $v_i^+ = 0$) as a function of its initial rotational levels, N_i^+, varying from 0 to 10.

($N_i^+ = 0 - 10$) rotational levels of its ground vibrational level ($v_i^+ = v_f^+ = 0$). The electron impact collision energies range between 0.01 and 300 meV. Convoluting these cross-sections conform equation (6), we obtain the DR, RE, and RdE thermal rate coefficients for electron temperatures ranging between 10 and 1000 K.

In Fig. 1, we show a typical behaviour of the DR ($N_i^+ = 0$, left-hand panel) and of the RE ($N_i^+ = 0 \rightarrow N_f^+ = 2$, right-hand panel) cross-sections and their thermal rate coefficients. In black, we represent the cross-sections as function of collision energy while in red we give the scaled rate coefficients as function of the electron temperature, the scaling factors being also given. In the left-hand panel, one can notice how the cumulation of the narrow constructive Rydberg resonances at about 6 meV will produce a maximum in the shape of the DR rate coefficient. The right-hand panel of the same figure gives us the general form of the RE rate coefficient, where the sharp threshold present in the cross-section is averaged out into a monotonically increasing function. Fig. 2 shows the rate coefficient for the consecutive $N_i^+ \rightarrow N_i^+ + 2$ excitations – allowed by the selection rules – for $N_i^+ = 0 - 10$ initial rotational quantum numbers. One can notice that their magnitudes are monotonically decreasing as N_i^+ is increased.

Contrary to this, the DR Maxwell rate coefficients shows a more complicated behaviour as function of electron temperature and target initial rotational quantum number, as one can see in Fig. 3. The rate coefficients obtained for the different initial rotational levels vary between one and two orders of magnitude as function of the electron temperature.

Up to 200 K, the most populated target rotational level (at local thermal equilibrium) gives the major contributions to the rate coefficient. Above this temperature the higher rotational quantum numbers become more and more important. Depending on the rotational quantum number of the initial state of the target, the rates show various temperature dependencies, from the smoothly decreasing behaviour to more general functions showing at least one maximum – see Fig. 1. While for low rotational quantum numbers the DR rate coefficients are exceeded by RE already at electron temperatures smaller than 50 K, for $N_i^+ = 10$ target this takes place at $T \sim 300$ K only.

The thermal rate coefficients obtained for the $N_i^+ \rightarrow N_f^+ = N_i^+ - 2$ RdEs of D_2^+ for $N_i^+ = 2$ to 10 and $v_i^+ = v_f^+ = 0$ are given in Fig. 4. The magnitude of rate coefficients increase with the initial rotational quantum numbers. It is also notable that below 1000 K, they are larger than those of the DR.

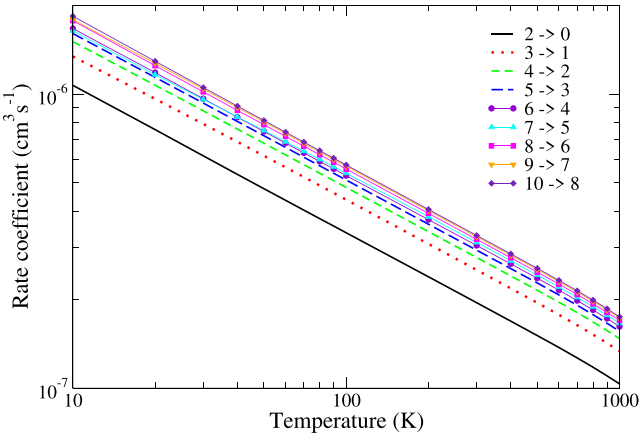

Figure 4. Maxwell rate coefficients for the RdE $N_i^+ \rightarrow N_f^+ = N_i^+ - 2$, with $N_i^+ = 2$ to 10 of the vibrationally relaxed ($v_i^+ = 0$) D_2^+ ($X\,^2\Sigma_g^+$).

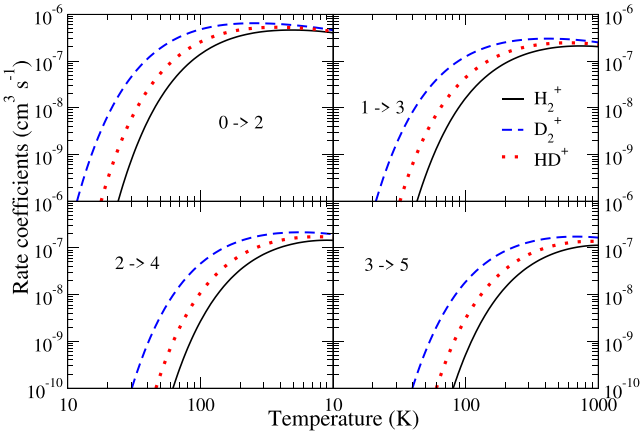

Figure 5. Isotopic effects in RE: Rate coefficients for $N_i^+ \rightarrow N_f^+ = N_i^+ + 2$ transitions, $N_i^+ = 0$ to 3, for the vibrationally relaxed $X^2\Sigma_g^+$ H_2^+, HD^+, and D_2^+ systems.

Table 1. Comparison of Maxwell rate coefficients (in cm^3 s^{-1}) for $N_i^+ \rightarrow N_f^+ = N_i^+ + 2$ REs of H_2^+, HD^+, and D_2^+ by collision with electrons at room temperature ($T = 300$ K).

N_i^+	H_2^+	HD^+	D_2^+
0	4.27473E-7	5.20549E-7	6.40280E-7
1	1.47448E-7	2.06564E-7	2.91847E-7
2	7.30450E-8	1.16444E-7	1.88170E-7
3	4.0060E-8	7.26357E-8	1.32346E-7
4	2.30159E-8	4.70647E-8	9.65611E-8
5	1.36503E-8	3.12933E-8	7.16222E-8
6	8.54116E-9	2.15608E-8	5.46144E-8
7	5.56954E-9	1.49720E-8	4.19320E-8
8	3.69408E-9	1.04648E-8	3.26509E-8
9	2.45815E-9	8.02520E-9	2.57048E-8
10	1.72925E-9	5.91376E-9	2.03948E-8

In Fig. 5, we compare the thermal rate coefficients for the RE from the lowest four rotational levels of H_2^+ (continuous black line), HD^+ (dotted red line), and D_2^+ (dashed blue line). The isotopic effects mainly due to the sharp thresholds are notable (notice the use of the logarithmic scale). We found that heavier the isotopologue, the larger the rate coefficient. This effect is quantified in Table 1 for the first eleven initial rotational levels of the targets for collisions taking place at $T = 300$ K temperature.

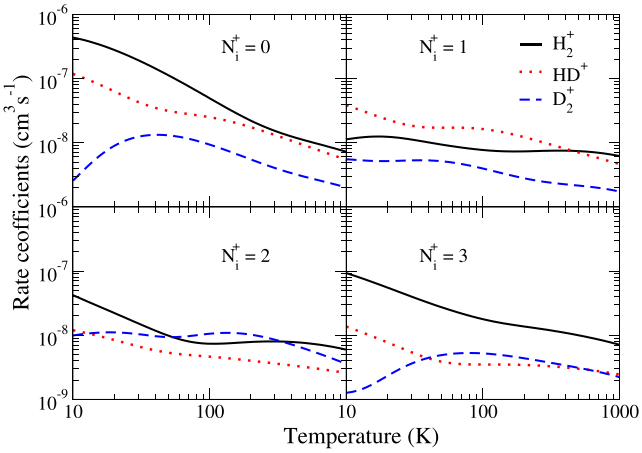

Figure 6. Isotopic effects in DR: Rate coefficients for $N_i^+ = 0$ to 3, for the vibrationally relaxed $X^2\Sigma_g^+$ H_2^+, HD^+, and D_2^+ systems.

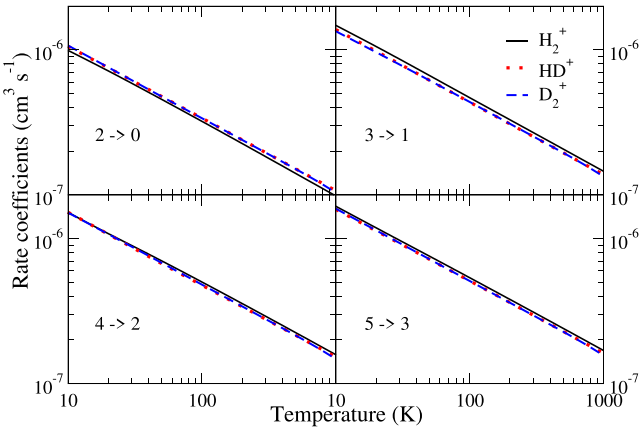

Figure 7. Isotopic effects in RdE: Rate coefficients for $N_i^+ \rightarrow N_f^+ = N_i^+ - 2$ transitions, $N_i^+ = 2$ to 5, for the vibrationally relaxed $X^2\Sigma_g^+$ H_2^+, HD^+, and D_2^+ systems.

Fig. 6 presents the isotopic effects obtained for DR for the lowest four rotational quantum numbers of the vibrationally relaxed target. Due to the very different dependence of the DR process on the initial and final channels with respect to the RE, we obtain different isotopic effects compared to those of Fig. 5. Except for $N_i^+ = 2$ case where the rate for D_2^+ is very close to that of H_2^+ and exceeds the one of HD^+ and for $N_i^+ = 3$ for $T = 40$–400 K, the rates obtained for the heaviest isotopologue are the smallest among all. The mass dependence of the cross-section and/or rate coefficients is complex. On one hand it is present in the position of the ro-vibrational levels and rotational/vibrational constants. Heavier the isotopologue, lower the ro-vibrational levels and smaller the level spacings. But the major part of the mass dependence we have via the Franck–Condon overlap of the initial/entrance and final/exit channels. This later is strongly depending on the molecular species.

Similarly to DR and RE, in Fig. 7 we have compared the RdE rate coefficients for the three isotopologues for the lowest four $\Delta N = -2$ transitions. The dependence of the RdE on the initial and final channels and the lack of threshold effects, in contrary to RE, lead to a slight isotopic effect.

Table 2. Fitting parameters for the equation (7), corresponding to the rate coefficients for DR of vibrationally relaxed D_2^+ on its lowest 11 rotational levels ($N_i^+ = 0 - 10$, $v_i^+ = 0$) with electrons of temperature in the range 10–1000 K.

N_i^+	a_0 ($cm^3\ s^{-1}$)	a_1	a_2 (K)	a_3 ($cm^3\ s^{-1}$)	a_4	a_5 (K)	RMS
0	1.61858E-9	− 0.026 610	1.350 36	2.97304E-9	− 1.389 79	57.3832	0.008 41
1	2.41400E-9	− 0.281 201	1.250 69	1.15502E-10	− 2.873 98	137.585	0.015 66
2	3.58811E-9	− 0.609 918	10.6046	1.24094E-8	− 1.411 35	264.577	0.009 77
3	6.49161E-10	0.092 753	− 8.572 27	3.73310E-9	− 0.674 586	54.0504	0.007 23
4	1.43940E-9	− 0.072 85	8.760 12	3.71294E-9	− 0.873 084	93.3021	0.011 35
5	5.20107E-9	− 0.804 386	15.7873	6.03106E-9	− 0.885 171	164.260	0.007 10
6	3.40860E-9	− 0.737 167	5.063 39	6.55842E-9	− 0.945 548	72.6807	0.006 01
7	1.56377E-9	− 0.662 548	4.609 87	6.96067E-9	− 0.800 087	73.4612	0.006 47
8	5.08388E-9	− 0.677 241	− 1.886 73	4.75096E-9	− 0.792 344	78.2720	0.007 83
9	7.44652E-9	− 0.615 038	1.939 63	3.35883E-9	− 1.079 090	140.250	0.008 43
10	4.02898E-9	− 0.531 062	3.935 37	8.19758E-9	− 0.827 386	54.8747	0.008 78

Table 3. Fitting parameters for the equation (8), corresponding to the rate coefficients for RdE $N_i^+ \rightarrow N_f^+ = N_i^+ - 2$ of vibrationally relaxed ($v_i^+ = 0$) D_2^+ on its rotational levels $N_i^+ = 2 - 10$ with electrons of temperature in the range of 10–1000 K.

N_i^+	a_0 ($cm^3\ s^{-1}$)	a_1	a_2 (K)	RMS
2	1.94131E-7	− 0.502 252	0.006 921	0.007 45
3	2.51942E-7	− 0.503 619	0.401 653	0.008 13
4	2.77168E-7	− 0.503 306	0.185 143	0.007 24
5	2.93427E-7	− 0.503 931	0.145 077	0.006 97
6	3.03986E-7	− 0.502 306	0.044 583	0.002 08
7	3.12123E-7	− 0.490 849	0.120 819	0.012 80
8	3.19233E-7	− 0.503 000	− 0.053 667	0.007 42
9	3.26264E-7	− 0.506 715	0.214 215	0.001 78
10	3.29173E-7	− 0.504 694	− 0.042 102	0.007 13

Table 4. Fitting parameters for the equation (8), corresponding to the rate coefficients for RE $N_i^+ \rightarrow N_f^+ = N_i^+ + 2$ of vibrationally relaxed ($v_i^+ = 0$) D_2^+ on its rotational levels $N_i^+ = 0 - 10$ with electrons of temperature between T_{min} and 1000 K, where T_{min} is the temperature below which the rate coefficient is lower than 10^{-14} $cm^3\ s^{-1}$.

N_i^+	T_{min} (K)	a_0 ($cm^3\ s^{-1}$)	a_1	a_2 (K)	RMS
0	10	9.80558E-7	− 0.510 696	128.209	0.024 27
1	11	5.98558E-7	− 0.528 565	215.309	0.062 29
2	16	5.16852E-7	− 0.541 313	302.347	0.096 60
3	20	4.88827E-7	− 0.560 415	390.647	0.143 60
4	25	4.80191E-7	− 0.582 399	479.527	0.183 99
5	29	4.77666E-7	− 0.603 300	567.434	0.213 97
6	33	4.81761E-7	− 0.624 484	651.362	0.235 55
7	37	4.87513E-7	− 0.645 269	734.352	0.249 84
8	41	4.96209E-7	− 0.666 460	814.971	0.258 15
9	45	5.07156E-7	− 0.687 319	893.630	0.261 11
10	49	5.17958E-7	− 0.709 294	969.819	0.256 49

In order to facilitate the use of our recombination, excitation and de-excitation rate coefficients for kinetic modelling, we have fitted their temperature dependence by using Arrhenius-type formulas.

For the DR we used

$$\alpha(T) = a_0 \left(\frac{T}{300}\right)^{a_1} e^{-\frac{a_2}{T}} + a_3 \left(\frac{T}{300}\right)^{a_4} e^{-\frac{a_5}{T}}, \quad (7)$$

and for the rotational transitions

$$\alpha(T) = a_0 \left(\frac{T}{300}\right)^{a_1} e^{-\frac{a_2}{T}}, \quad (8)$$

where T is in Kelvin and α in $cm^3\ s^{-1}$. The fitting parameters for the DR of the lowest 11 rotational levels of the target, the 9 RdE, and 11 RE rate coefficients are summarized in Tables 2, 3, and 4. For all the processes, the fitted values reproduce well our MQDT rate coefficients, according to the RMS values given in the fourth column of each table in the whole temperature range of $10 < T < 1000$ K.

In addition to the consecutive transitions we have also calculated the rate coefficients for rotational transitions with $\Delta N^+ = 4$. We have found that they are about two orders of magnitude smaller than those obtained for $\Delta N^+ = 2$ for the same initial rotational quantum number. Consequently, we have omitted them from this paper. And finally, besides the symmetry allowed $\Delta N^+ = 2$, 4 rotational transitions of the H_2^+ and D_2^+ cations one has to mention that the $\Delta N^+ = 1$ rotational transitions in HD^+ are significant due to the existing permanent dipole moment ($\mu = 0.85$ Debye; Shafir et al. 2009). The theoretical treatment of these transitions due to the inexistent 'gerade–ungerade' couplings is a serious challenge.

4 CONCLUSIONS

In the framework of the stepwise MQDT, we have calculated cross-sections between 0.01 meV and 0.3 eV, and consequently thermal rate coefficients between 10 and 1000 K, for DR and RE/RdE of electrons with $D_2^+(X^2\Sigma_g^+)$ ions for their lowest 11 rotational levels and in their ground vibrational level $v_i^+ = v_f^+ = 0$.

In our model, we have accounted for all relevant electronic states and symmetries of the cation target, for all relevant rotational and vibronic electronic couplings, by taking into account the quantum interference among the direct and indirect mechanisms.

The obtained rate coefficients show strong dependence on the initial rotational state of the molecular target.

We have compared these DR and RE/RdE coefficients obtained for D_2^+ with similar rate coefficients previously calculated for H_2^+ and HD^+ isotopologues. They crucially depend on fine balance between the initial and final channels and threshold effects. For RE we observe that heavier the cation, larger the rate coefficient, while for RdE we get only a slight isotopic effect. The strongest initial/final channel dependence can be observed for the DR. The obtained isotopic differences clearly put in evidence the importance of the present results especially for kinetic modelling of the environments where deuterated species are present.

These results complement significantly the recent investigations on the other main competing destructive channels of H_2^+, HD^+, and D_2^+ via their reactions with H_2, HD, and D_2 that produce the H_3^+, H_2D^+,

D_2H^+, and D_3^+ triatomic ions (Merkt, Hövler & Deiglmayr 2022), allowing to remove significant uncertainties of previous studies.

The numerical data, ready to be used in the kinetic modelling in astrochemistry and cold plasma physics will be available upon request.

ACKNOWLEDGEMENTS

The authors acknowledge support from Fédération de Recherche Fusion par Confinement Magnétique (CNRS and CEA), La Région Normandie, FEDER, and Labex EMC3 via the projects PTOLEMEE, Bioengine COMUE Normandie Université, the Institute for Energy, Propulsion and Environment (FR-IEPE), the European Union via COST (European Cooperation in Science and Technology) actions TUMIEE (CA17126), MW-Gaia (CA18104), and MD-GAS (CA18212), and from the l'Agence Universitaire de la Francophonie en Europe Centrale et Orientale (AUF ECO) via the project CE/MB/045/2021 CiCaM - ITER'. The authors are indebted to Agence Nationale de la Recherche (ANR) via the project MONA. This work was supported by the Programme National 'Physique et Chimie du Milieu Interstellaire' (PCMI) of INSU, CNRS with INC/INP co-funded by CEA and CNES. J.Zs.M. thanks the financial support of the National Research, Development and Innovation Fund of Hungary, under the FK 19 funding scheme with project no. FK 132989.

DATA AVAILABILITY

The data underlying this article will be shared on reasonable request to the corresponding author.

REFERENCES

Andersen L. H., Johnson P. J., Kella D., Pedersen H. B., Vejby-Christensen L., 1997, Phys. Rev. A, 55, 2799
Auerbach D., Cacak R., Caudano R., Gaily T. D., Keyser C. J., McGowan J. W., Mitchell J. B. A., Wilk S. F. J., 1977, J. Phys. B, 10, 3797
Chakrabarti K. et al., 2013, Phys. Rev. A, 87, 022702
Djuissi E. et al., 2020, Rom. Astron. J., 30, 101
Epée Epée M. D., Mezei J. Zs. Motapon O., Pop N., Schneider I. F., 2016, MNRAS, 455, 276
Faure A., Tennyson J., 2001, MNRAS, 325, 443
Faure A., Tennyson J., 2002, J. Phys. B, 35, 3945
Faure A., Tennyson J., 2003, MNRAS, 340, 468
Faure A., Kokoouline V., Greene C. H., Tennyson J., 2006, J. Phys. B, 39, 4261
Galli D., Palla F., 2013, ARA&A, 51, 163
Gay C. D., Stancil P. C., Lepp S., Dalgarno A., 2011, ApJ, 737, 44
Giusti-Suzor A., 1980, J. Phys. B, 13, 3867
Hus H., Yousif F., Noren C., Sen A., Mitchell J. B. A., 1988, Phys. Rev. Lett., 60, 1006
Kashinski D. O., Talbi D., Hickman A. P., Di Nallo O. E., Colboc F., Chakrabarti K., Schneider I. F., Mezei J. Zs., 2017, J. Chem. Phys., 146, 204109
Kokoouline V., Faure A., Tennyson J., Greene C. H., 2010, MNRAS, 405, 1195
Kolos W., Wolniewicz L., 1969, J. Chem. Phys., 50, 3228
Krohn S. et al., 2000, Phys. Rev. A, 62, 032713
Krohn S., 2001, PhD thesis, Univ. Heidelberg
Lepp S., Shull M., 1984, ApJ, 280, 465
Merkt F., Höveler K., Deiglmayr J., 2022, J. Phys. Chem. Lett, 13, 864
Mezei J. Zs. et al., 2019, ACS Earth Space Chem., 3, 2376
Motapon O., Waffeu Tamo F. O., Urbain X., Schneider I. F., 2008, Phys. Rev. A, 77, 052711
Motapon O. et al., 2014, Phys. Rev. A, 90, 012706
Orlikowski T., Staszewska G., Wolniewicz L., 1999, Mol. Phys., 96, 1445
Schneider I. F., Strömholm C., Carata L., Urbain X., Larsson M., Suzor-Weiner A., 1997, J. Phys. B, 30, 2687
Schwalm D. et al., 2011, J. Phys.: Conf. Ser., 300, 012006
Seaton M. J., 1983, Rep. Prog. Phys., 46, 167
Shafir D. et al., 2009, Phys. Rev. Lett., 102, 223202
Staszewska G., Wolniewicz L., 2002, J. Mol. Spectrosc., 212, 208
Telmini M., Jungen Ch., 2003, Phys. Rev. A, 68, 062704
Tennyson J., 1996, At. Data Nucl. Data Tables, 64, 253
Waffeu Tamo F. O. et al., 2011, Phys. Rev. A, 84, 022710
Wolniewicz L., Dressler K., 1994, J. Chem. Phys., 100, 444

This paper has been typeset from a TEX/LATEX file prepared by the author.